FSI within Aortic Arch Model over Cardiac Cycle and Influence of Wall Stiffness on Wall Stress in Layered Wall

F. Gao and T. Matsuzawa

***Abstract*—The aorta is the largest artery that delivers blood from the heart to the rest of the body, and many cardiovascular diseases often occur on the aortic arch. The complex mechanical interaction between pulsatile blood flow and wall dynamics in the aortic arch model was simulated by means of computational loose coupling fluid-structure interaction analyses. This study investigates the pulsatile flow field in the aortic arch, shows the wall displacement and aorta deformation over cardiac cycle, determines wall stresses, evaluated the influence of wall stiffness, and provides physical insight into the biomechanics of aortic dissection. The numerical layered aortic model may prove useful for studying biomechanical analysis and the pathogeneses of aortic dissection.**

***Index Terms*—Wall stiffness, Aortic wall, Aortic dissection**

I. Introduction

Aortic dissection and dissecting aneurysm are a pathological state in which a tear develops in the intima layer of the aorta, the blood enters at the site of the tear, separates layers of aorta, and spreads the dissection. Aortic dissection and dissecting aneurysm often occur on the aortic arch and aortic dissection is the commonest catastrophe affecting the aorta, occurring more frequently than rupture [1]. An understanding of the pathophysiologic mechanisms of cardiovascular diseases has the potential to help direct therapeutic options. The numerically simulating the flow in blood vessels could understand the development of many diseases [2] and the flow structure in the aortic arch has been widely studied in the past [3, 4, 5]. Aortic wall rupture and tear is a phenomenon that occurs when the mechanical stress acting on the wall exceeds is failure strength [6,7]. The dynamic interaction of aortic wall with blood flow plays an important role in the cardiovascular system. The quantification of the hemodynamics is essential for the characterization of biomechanical environment. There have been several computational studies of fluid-structure interaction in the aortic valve [8], aortic aneurysm [9], and in stented aneurysm models [10]. These studies have provided great insight into the complexity of interaction between flow patterns and aortic wall. However the interaction between blood flow and the aortic wall in an aortic arch model has not yet been studied.

In this work we describe the complex interaction of pulsatile flow and the aortic arch wall by using the loosely-coupled algorithms and the stress analysis in aortic arch wall.

Prior works showed that arterial stiffness is an important determinant of cardiovascular risk [11]. The main structural alterations at the site of the large artery media account for arterial stiffening [12]. We also investigate the influence of medial stiffness on stress distribution across the aortic wall.

We performed the computational analyses to investigate the flow field, wall deformation, stress distribution, and influences of wall stiffness on wall stress within aortic arch model.

Manuscript received April 15, 2006. This work is conducted as a program for the "Fostering Talent in Emergent Research Fields" in Special Coordination Funds for Promoting Science and Technology by Ministry of Education, Culture, Sports, Science and Technology.

F. Gao is with Japan Advanced Institute of Science and Technology, Ishikawa, 923-1292, Japan. (tel: (81)761-51-1699; fax: (81)761-51-1305; e-mail: feng-g@ jaist.ac.jp, fgao_2002@163.com).

T. Matsuzawa is with Center for Information Science, Japan Advanced Institute of Science and Technology, Ishikawa, 923-1292, Japan.

II. Method

A. Geometry

Computer models of an aortic arch were generated with commercial software (GAMBIT v. 2.0; Fluent Inc., NH, USA) such that the radius of the arch was set to 3.0 cm and the diameter of vessel was assumed to be 2.0 cm, as has been shown to be typical [13]. The aortic arch model is shown in Fig. 1. The thickness of whole wall was chosen to be 2mm [14, 15]. In this three-layeredwall model, the thickness ratio of intima/media/adventitia was set at 1/6/3 based on Schulze-Bauer's [16] observations. Therefore, the thickness of intima, media, and adventitia were t_i=0.2mm, t_m=1.2mm, and t_a=0.6mm, respectively. The most important location of the aortic arch is the outer wall of the arch, from the right lateral aortic wall downstream along the greater curvature of the arch. Arch angle α is defined so that the wall position of outer wall can be discussed. The arch angle α is measured at the circumference of the median longitudinal cross-section, and ranges from 0° and 180°.

B. Fluid-structure Coupling Analysis

The impact of blood flow on the aortic wall and the deformation of the wall affects the flow field. We used the technique known as fluid structure interaction to compute the wall stresses in our aortic arch model. The fluid structure interaction (FSI) algorithm treats the equations that solve the structural problem, the remeshing problem, and the fluid problem by a staggered approach; that is to say, the algorithm solves the equations in sequence. First, the equations governing

the fluid are solved for fluid velocity and pressure fields. Subsequently the traction, i.e., pressure and viscous stress, is calculated at the interface between fluid and structure. The traction is then applied to the structure together with the other boundary conditions, and the structural equations are solved for the displacement of the structure. At this point the position of the wetted surface is updated. Finally, the equations that describe the mesh displacement are solved by imposing the displacement of the wetted surface as a boundary condition. This cycle is repeated until convergence is achieved. The finite element method (FEM) was utilized for all the computational studies reported in this work. The code *Fidap* (Fluent Inc., Lebanon, NH) has been used to carry out the simulation.

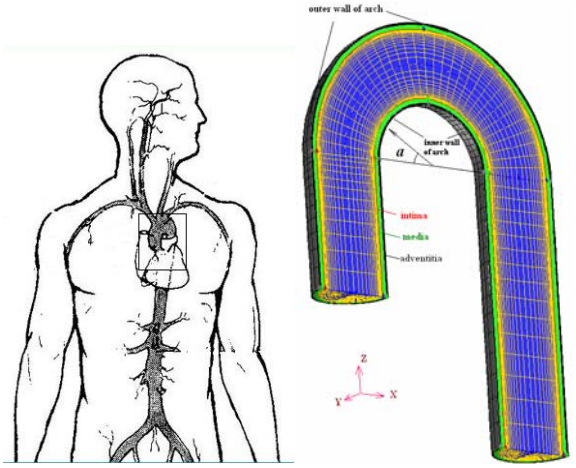

Fig.1. Three-layered aortic arch model. R represents the radius of the arch. The angle ***α*** represents the wall position in the median longitudinal cross-section.

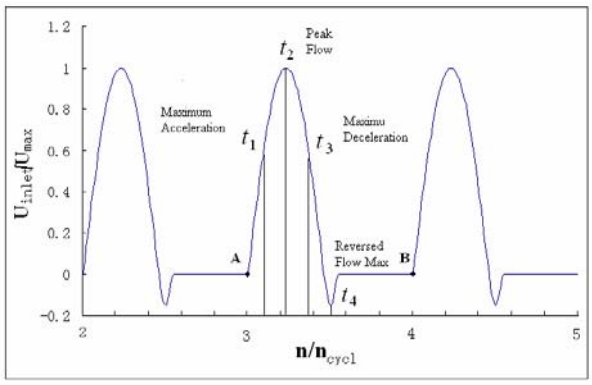

Fig.2. Inlet velocity profile. N is the time step, n_{cycl} is the total time steps in one cycle. For the final run, the cardiac cycle is started at A and ends at B.

The Young's modulus of the media was set three times larger than that of the adventitia according experimental results reported by Xie et al. [17]. The elasticity of the intima was less than that of the media based on Fischer's [18] experimental data. In this study, the Young's modulus of the intima was assumed to be the same as that of the adventitia. The mean Young's modulus of the vessel wall across whole wall volume is same and we assume that the Young's modulus of each layer is inverse proportion to the area of the layer in the cross section. The mean Young's modulus was set 1.5MPa.

The fluid is incompressible and Newtonian with a viscosity of 0.0035 Pa·s and a density of 1050 kg/m^3. At the aortic inlet, a flat flow velocity profile was used together with pulsatile waveform based on reported experimental data by Pedlety [19]. This waveform is shown in Fig.2. The assumption of a flat velocity profile at the aortic inlet is justified by in vivo measurements using hot film anemometry on various animal models that have demonstrated that the velocity profile distal to the aortic valve are relatively flat, Nerem[20]. In our calculations, the Reynolds number is fixed at ***Re***=4000 based on the inlet velocity at peak systole of the cardiac cycle. At the aortic outlet, a zero pressure condition was applied. The simulation reached nearly steady-state oscillation after approximately third cycle. The fourth cycle was used as the final periodic solution and it is presented in this paper. The surface of the aortic inlet and aortic outlet are fixed in all directions. The other outer surface of the aortic model was taken as load free.

III. Result

A. Velocity

A very important aspect of analysis results is the flow field in the aortic arch. Fig.3 shows that the flow pattern in median longitudinal cross-section of aortic arch at selected times. Four consecutive cardiac times were selected to characterize the interaction between blood flow and wall (Fig.2). Label t_1 denotes the max acceleration, t_2 the peak flow, t_3 the max deceleration, t_4 the peak reverse flow.

Fig. 3(a) shows that the flow at max acceleration (t_1) at the entrance to arch portion is skewed toward the inner aortic wall. This vortical type flow pattern is induced by the curved geometry, and it is not a result of the flat inlet condition. The results at peak flow (t_2) and max deceleration (t_3) (Fig. 3(b) and (c)) demonstrate that, after the top of arch, skewing of the velocity distribution reversed, and the location of maximum velocity shifted towards the outer wall of aortic arch. Fig. 3(d) shows that flow pattern in the aorta at peak reverse flow. Retrograde flow in the aorta at this point of cycle likely provides blood flow to the coronary arteries. The flow pattern exhibits skewness and the velocity is skewed towards the inner wall of aortic arch, which is completely from that at other points in the cardiac cycle.

The curvature of aortic arch is expected to induce significant secondary flow within aorta. Fig.4 demonstrates the secondary flow for the aortic cross-sections at peak flow. The outer wall is located on the left hand side in Fig. 4. The secondary flow was almost symmetrical at all cross-section of aorta. At the entrance of ascending portion (Fig.4 (a)), the secondary flow is from the outer to the inner wall. The cross-section in Fig.4 (b), (c), and (d) are located in the arch angle ***α***=45, 90, and 135. Some of secondary flow is from the inner to outer wall, and there is another cross-flow developing toward the inner wall near aortic

wall. A strong clockwise-rotating vortex developed on left-hand side of the cross-section at ***a***=90 and 135.

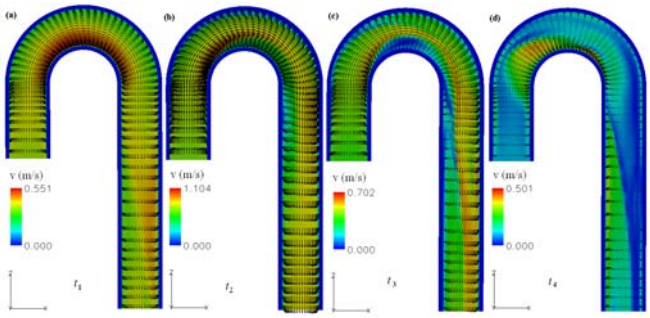

Fig. 3 Velocity vectors at the median cross-section in the aortic arch model at (a)t_1 (Max acceleration), (b) t_2 (Peak flow), (c)t_3 (Max deceleration), and (d) t_4 (Reversed flow max) in the pulse cycle.

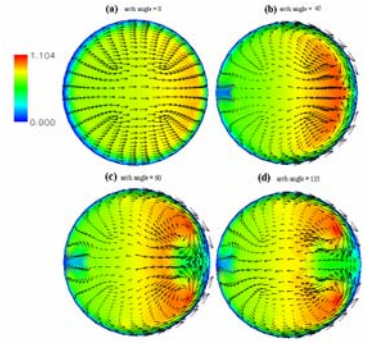

Fig. 4 Secondary flow at cross section in aortic arch at (a) *a*=0, (b) *a*=45, (c) *a*=90, and (d) *a*=135 position at t_2 (peak flow)

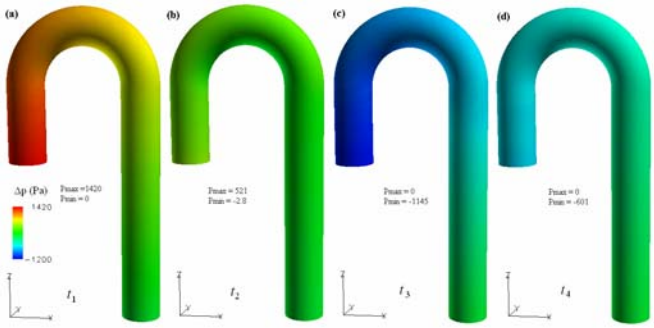

Fig.5 Fluid pressure at the wall at (a) t_1 (Max acceleration), (b) t_2 (Peak flow), (c)t_3 (Max deceleration), and (d)t_4 (Reversed flow max) in the pulse cycle.

B. Wall Pressure

The wall dynamic pressure contours are presented in Fig. 5. The pressure is the relative pressure induced by blood flow since we set the zero pressure at outlet and outer side of wall. At max acceleration (Fig. 5(a)), the pressure is maximum at inlet of aorta. Low pressure region is the outlet of aorta. The pressure in outer wall of arch is higher than that in inner wall of arch. Fig. 5(b) shows that the wall pressure distribution has the same pattern as that of max acceleration, but the magnitude of the pressure is much reduced. The relative pressure at inlet of aorta becomes negative value at max deceleration (Fig. 5(c)) and the negative pressure value is reduced at peak reverse flow (Fig. 5 (d)). The relative pressure distribution has been induced by the flow and acceleration. The lager acceleration leads to the larger fluid pressure.

C. Wall Placement

Fig. 6 shows the displacement vector for the aortic wall at four selected times. At max acceleration (Fig.6 (a)), the displacement of aorta is towards the left side of arch (ascending aorta side). The maximum displacement is at the distal to the arch portion, which is due to the fixed condition of both at inlet and outlet. The displacement is reduced and towards the top side of arch at peak flow (Fig.6 (b)). At max deceleration (Fig.6 (c)), the direction of displacement vector is reversed towards the right side of arch (descending aorta side). The displacement of aorta wall is reduced at peak reverse flow (Fig.6 (d)).

Due to the highly unsteady and three-dimensional nature of blood flow in the aorta, it should be investigate the variation of displacement over the cardiac cycle. For reduction of the effects of the boundary condition (fixed at inlet and outlet), only the arch portion was selected to show the variation of displacement of aortic wall. Fig. 7 shows the displacement of outer wall, inner wall, and side wall of aortic arch potion over one cardiac cycle. For the value of displacement in Fig.7, the displacement denotes the moving distance from original position in radial direction of arch for outer wall and inner wall of arch, in axial direction of arch for side wall of arch. It is specified that the positive value is towards the outer of the arch for the outer wall and inner wall; it is specified that the positive value is towards the outside of lumen for side wall.

During systole acceleration phase, the displacement is towards the outer of the arch in ascending portion and towards the inner of the arch in descending portion for the outer wall and inner wall (Fig. 7(a)(b)). During systole deceleration phase, the direction of displacement reverses both in ascending portion and descending portion. For the side wall of arch (Fig. 7(c)), the direction of displacement is towards the outside of lumen during systole acceleration phase and towards the inside of lumen during systole deceleration phase. In outer wall, inner wall, and side wall of arch, the high displacement appears at max acceleration and max deceleration. Another high displacement appears at retrograde flow. During the diastole phase, the high displacement appears in turn at ascending portion and descending portion. The displacement is higher at ascending portion than that at descending portion for the side wall of arch.

Under the effect of blood flow, the aorta deformation is induced by the displacement of aortic wall. Based on the wall displacements, Fig.8 shows the aorta deformation in the arch radial direction and the arch axial direction along the arch over on cardiac cycle. The aorta deformation is expressed by the changes of the aorta diameter in the arch radial direction and the arch axial direction.

Fig. 8 shows that the high deformation is at max acceleration and max deceleration. The large deformation in arch radial direction (Fig.8 (a)) is at descending portion during systole

acceleration phase and at ascending portion during systole deceleration phase. The large deformation in arch axial direction (Fig.8 (b)) is at ascending portion at max acceleration and max deceleration. Another large deformation appears at reverse flow. It should be noted that the deformation in arch axial direction is very different from that in arch radial direction. Furthermore the value of deformation in axial direction is larger than that in arch radial direction, so the section of wall becomes elliptical.

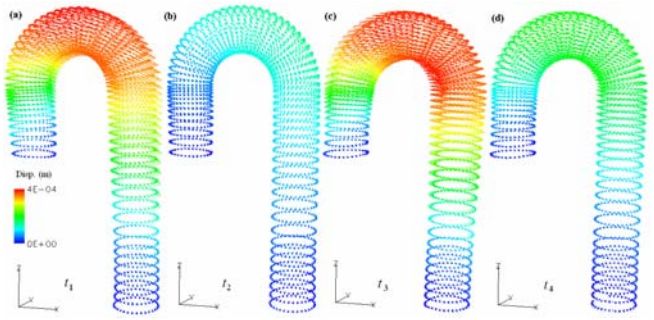

Fig.6 Displacement at the wall at (a) t_1 (Max acceleration), (b) t_2 (Peak flow), (c)t_3 (Max deceleration), and (d)t_4 (Reversed flow max) in the pulse cycle.

(a) (b)

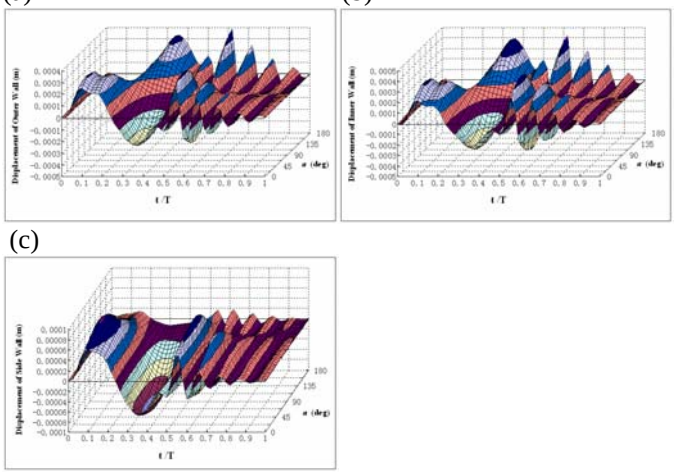

(c)

Fig.7 Displacement at (a) outer wall of arch, (b) inner wall of arch, and (c) side wall of arch over one cardiac cycle.

(a) (b)

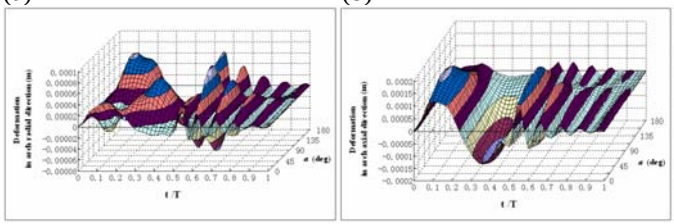

Fig. 8 Deformation of aorta (a) in arch radial direction and (b) in arch axial direction over one cardiac cycle.

D. Wall Stress

Fig. 9 presents the variations of the circumferential stress, the longitudinal stress, and the radial stress in outer wall along arch portion during the cardiac cycle. The stresses are averaged across the aortic wall thickness. The circumferential stress, the longitudinal stress, and the radial stress in outer wall initially increases at the systole acceleration phase and then decreases during the deceleration phase and then there is a transient increase at the reverse flow. The circumferential stress (Fig. 9(a)) decreases along the arch. The longitudinal stress (Fig. 9(b)) along the arch gets the peak values at the entrance ascending portion, the top of the arch and the distal end of arch. The radial stress (Fig. 9(c)) along the arch gets a peak value at the mid ascending portion and the mid descending portion.

(a) (b)

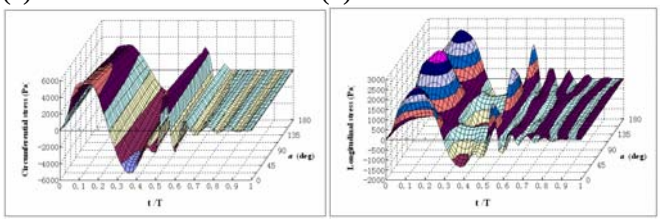

(c)

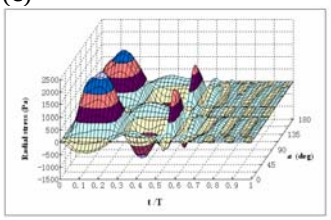

Fig. 9 Wall stress distribution (a) Circumferential stress, (b) Longitudinal stress, and (c) Radial stress) in outer wall of arch over one cardiac cycle.

E. Effect of Wall Stiffness on Wall Stress

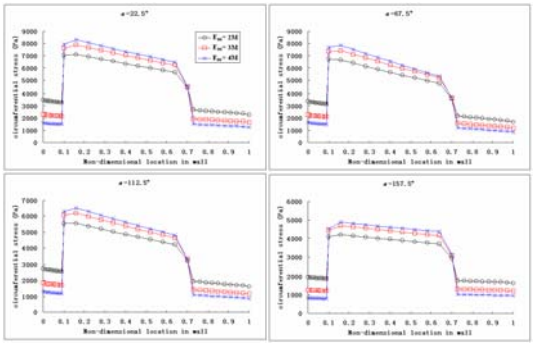

Fig. 10. Effect of medial stiffness on variation of the circumferential stress across the wall

For investigate the effect of medial stiffness on wall stress across wall thickness, the Young's modulus of the intima and adventitia were kept constant ($\boldsymbol{E_i}$ = 1.0MPa, $\boldsymbol{E_a}$ = 1.0MPa), and the Young's modulus of the media varied from 2MPa to 4MPa.

The outer wall of the arch is an important position in aortic arch model. Four positions – a=22.5º, a=67.5º, a=112.5º, and a=157.5º – were selected in the outer wall of the arch to illustrate the variation of stresses across the wall. Since the stress at acceleration phase is high, max acceleration time were selected to characterize in detail the variations of stresses.

The effects of medial stiffness on the variation of circumferential, longitudinal, and radial stress are shown in Fig. 10, Fig. 11, and Fig. 12. The stresses in the media are higher, reaching a peak value in the media near the adventitia across the wall. Medial stiffness was found to have similar effects on

the variation of circumferential, longitudinal, and radial stress across the wall. Increasing the medial stiffness increases wall stress in the media while causing a decrease in stress in the intima and adventitia. As the medial Young's modulus becomes larger, the stress is greater in the media while smaller in the intima and adventitia. The peak stress along the arch portion was found to be markedly affected by the change in medial stiffness.

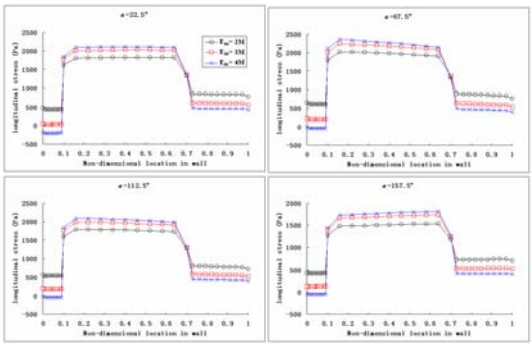

Fig. 11 Effect of medial stiffness on variation of the longitudinal stress across the wall

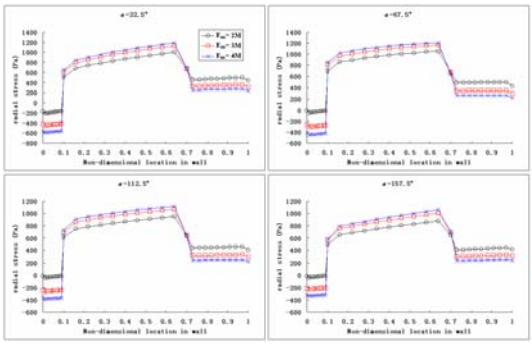

Fig. 12 Effect of medial stiffness on variation of the radial stress across the wall

IV. Discussion and Conclusion

This study was undertaken to gain understanding of the time-dependent complex mechanical interaction between blood flow and wall dynamics in a three-layered aortic arch model by means computational coupled fluid-structure interaction analyses.

The results of the simulations have revealed a flow field that is largely similar to that previously reported in a number of experimental studies [3-5]. It demonstrates that the results of the simulations are creditable. One of the advantages of previous studies is that their model included the branches of aorta. This study was concerned mainly with the effects of the arch of aorta on the fluid-structure interaction. Therefore, the three branches along the top of the aortic arch were not included in the model. In the future investigations, the branches will be added to the FSI model to improve physical approximations and models that capture the proper fluid physics and biology.

The pressure in blood includes atmospheric pressure and the pressure generated by the heart. There also is atmospheric pressure outside of the blood vessel. The transmural pressure, $P_{tm} = P_{inside} - P_{outside}$, can contribute to the deformation of the aortic wall. The blood vessel experiences the negative tranmural pressure. [19] This study investigated the relative pressure distribution under pulsatile blood flow. The variation of the relative pressure with time agrees with the previous study [21]. The amplitude of relative pressure (2.6kPa) over pulse cycle was a little larger than that (2.2kPa) in Tyszka's work[21]. The difference is due to the reference point. Our reference point is more far from the arch.

Wall deformations in aortic arch are completely different from straight vessel. Under the effect of blood flow, the cross-section of aorta could not keep circle as the straight vessel and it becomes elliptical. Geometry has been well established as a contributing factor to wall deformation, independently of the heterogeneity of the wall [22]. Our results demonstrated the detailed time-dependent presentation of wall displacement and wall deformation, and this detail can be used in future studies to determine the important biological significance.

During one cardiac cycle, the stresses in aortic arch wall are changeful, due to the time-dependent fluid flow and the arch structure. Wall stress is an important factor in aortic dissection, which has been recently addressed by several authors [6, 7, 23]. In the present study, the wall stress depicted in Fig. 9 is high at systolic acceleration phase. So during the cardiac cycle the systolic acceleration phrase is critical for risk of wall tear or dissection. Thubrikar et al. [6] have proposed that longitudinal stress could be responsible for transverse tears in the aortic dissection. Roberts [24] reported that the tear is located about at the entrance to the ascending portion of the arch and near the top of the arch. The longitudinal stress also peaks in the distal end of the arch, and tears do not often occur at this location. Circumferential stress and longitudinal stress should be considered together for understanding of the intimal tear [7]. The radial stress is a positive value in the ascending and descending portions, and thus, by definition, is tensile stress. Under normal conditions, radial stresses are compressive. MacLean et al. [23] showed that the aorta tore radially at a much lower value of radial tensile stress and mentioned that once a false lumen is formed by a dissection, radial tensile forces must exist in the aortic wall. In the present study, radial tensile stress exists due to the structure of arch and deformations of the wall.

Okamoto et al. [25] used a thick-walled cylindrical model of aorta to predict in vivo distensibility and wall stress distribution. Their results showed that mean circumferential stress did not vary significantly with age or patient group. Beller et al. [26] built a finite element model of the aortic arch for stress analysis. The results showed that stiffening the aorta to simulate aging did not markedly increase the averaged stresses in the aortic wall. Our results agree with theirs regarding the influence of stiffening on the mean stresses. However, they did not show the stress distribution across the wall thickness. The aortic wall consists of the intima, media, and adventitia, i.e., it is a multi-layered organ. The material properties of each layer can affect the stress distribution across the aortic wall. The stress

can not be distributed uniformly through the wall thickness. We extended these previous studies by considering stresses that were not averaged stresses, but rather were through the three-layered aortic wall. Our results indicate that the stress distribution across the aortic wall was not affected by the mean wall stiffening, while medial stiffening increased the stresses in the media and peak stress in the aortic wall. As medial stiffness increases, the medial stresses increase. This may increase the risk of dissection in the media. Higher stiffness of carotid wall material and circumferential wall stress were found in spontaneous cervical artery dissection patients [15]. As pointed out by Angouras et al. [27], impairment of vasa vasorum flow results in an aorta that is significantly stiffer, contributing to the development of aortic dissection. Thus sites of the aorta with stiffening may undergo higher wall stresses, which would have an influence on risk of aortic dissection.

Despite the more accurate predictions of aortic arch biomechanics utilizing an FSI methodology, there are additional limitations to the present study. Among these are neglecting of branches of arch, the assumption of a linear elastic modulus for modeling wall mechanical properties, the approximation of wall thickness, the anisotropic characterization of the tissue models, the absence of external forces induced by surrounding tissue and organs. The constant improvement in technology will allow us to add these additional complexities to the simulation capability.

A significant contribution of the present study is the investigation of the complex interaction between pulsatile blood flow and aortic wall within three-layered aortic model. This study investigates the pulsatile flow field in the aortic arch, shows the wall displacement and aorta deformation over cardiac cycle, determines wall stresses, evaluated the influence of wall stiffness, and provides physical insight into the biomechanics of aortic dissection. To the authors' knowledge, this is the first computation FSI study of 3-layered aortic arch model. Incorporating the branches into the aortic arch model as well as more realistic geometry, will be performed in the future work.

ACKNOWLEDGMENT

This research is conducted as a program for the "Fostering Talent in Emergent Research Fields" in Special Coordination Funds for Promoting Science and Technology by Ministry of Education, Culture, Sports, Science and Technology.

REFERENCES

[1] H.J. Safi and A.L. Estrera, "Aortic dissection", *British Journal of Surgery*, 91, 2004, pp. 523-525

[2] M.S. Moayeri, G.R. Zendehbudi, "Effects of elastic property of the wall on flow characteristics through arterial stenoses". J. Biomech. vol.36, 2003, pp.525-535.

[3] S. Endo, Y. Sohara, T. Karino, "Flow patterns in dog aortic arch under a steady flow condition simulating mi-systole". Heart Vessels vol.11, 1996, pp.180-191.

[4] N. Shahcheraghi, H.A. Dwyer, A.Y. Cheer, A.I. Barakat, T. Rutaganira, "Unsteady and three-dimensional simulation of blood flow in the human aortic arch". J. Biomech. Eng. vol.124, 2002, pp.378-387.

[5] H. Liu, "Multi-scale computation in hemodynamics", RIKEN symposium 2002.

[6] M.J. Thubrikar, P. Agali, F. Robicsek, "Wall stress as a possible mechanism for the development of transverse intimal tears in aortic dissections". J. Med. Eng. Tech. vol.23, 1999, pp.127-134.

[7] C.J. Beller, M.R. Labrosse, M.J. Thubrikar, F. Robicsek, "Role of aortic root motion in the pathogenesis of aortic dissection". Circulation vol.109, 2004, pp.763-769

[8] J.D. Hart, G.W.M. Peters, P.J.G. Schreurs, F.P.T. Baaijens, "A three-dimensional computational analysis of fluid-structure interaction in the aortic valve". J. Biomech. vol.36, 2003, pp.103-112.

[9] E.S. Di Martino, G. Guadagni, A. Fumero, G. Ballerini, R. Spirito, P. Biglioli, A. Redaelli, "Fluid-structure interaction within realistic three-dimensional models of the aneurysmatic aorta as a guidance to assess the risk of rupture of the aneurysm", Med. Eng. Phys. vol.23, 2001, pp.647-655.

[10] Z. Li, C. Kleinstreuer, "Blood flow and structure interactions in a stented abdominal aortic aneurysm model". Med. Eng. Phys. vol.27, 2005, pp.369-382.

[11] J. Blacher, G.M. London, M.E. Safar, "Influence of age and end-stage renal disease on the stiffness of carotid wall material in hypertension". J Hypertens. vol.17, 1999, pp.237–244.

[12] A. Benetos, "Pulse pressure and arterial stiffness in type 1 diabetic patients". Journal of Hypertension. 21(11), 2003, pp.2005-2007.

[13] D. Mori, K. Tsubota, S. Wada, T. Yamaguchi, "Concentrated high wall shear stress due to the torsion of the aortic arch and development of the aortic aneurysm", 2003 Summer Bioengineering Conference, June 25-29, Florida

[14] W.F., Ganong, Review of Medical Physiology, Lange Medical Publications, 1963

[15] S. Shiotani, M. Kohno, N. Ohashi, K. Yamazaki, H. Nakayama, Y. Ito, K. Kaga, T. Ebashi and Y. Itai, "Hyperattenuating Aortic Wall on Postmortem Computed Tomography", Radiation Medicine, 20(4), 2002 pp.201-206.

[16] C.A. Schulze-Bauer, C. Morth, G.A. Holzapfel, "Passive Biaxial Mechanical Response of Aged Human Iliac Arteries", J. Biomech. Eng. 125(3), 2003, pp.395-406.

[17] J. Xie, J. Zhou and Y.C. Fung, "Bending of Blood Vessel Wall: Stress-strain Laws of the Intima-media and Adventitial Layers", J. Biomech. Eng., 117, 1995, pp.136-145.

[18] E.I. Fischer, R.L. Armentano, F.M. Pessana, S. Graf, L. Romero, A.I. Christen, A. Simon and J. Levenson, "Endothelium-dependent Arterial Wall Tone Elasticity Modulated by Blood Viscosity", Am. J. Physiol. Heart Circ. Physiol., 282, 2002, pp.389-394.

[19] T.J. Pedley, The Fluid Mechanics of Large Blood Vessels, Cambridge University Press, 1980

[20] R.M. Nerem, ''Vascular Fluid Mechanics, the Arterial Wall, and Atherosclerosis,''J. Biomech. Eng., 114, 1992, pp. 274–282.

[21] J.M. Tyszka, D.H. Laidlaw, J.W. Asa, J.W. Silverman, "Three-dimensional, time-resolved (4D) relative pressure mapping using magnetic resonance imaging". J. Magn. Reson Imaging vol.12, 2000, pp.321-329

[22] C.M. Scotti, A.D. Shkolnik, S.C. Muluk and E.A. Finol, "Fluid-structure interaction in abdominal aortic aneurysms: effects of asymmetry and wall thickness", BioMedical Engineering OnLine, 2005, 4:64

[23] N.F. MacLean, N.L. Dudek and M.R. Roach, "The Role of Radial Elastic Properties in the Development of Aortic Dissections", J. Vasc. Surg., Vol.29, 1999, pp.703-710.

[24] W.C. Roberts, "Aortic Dissection: Anatomy Consequences and Causes", Am. Heart J., Vol.101, 1981, pp.195-214.

[25] R.J. Okamoto, H. Xu, N.T. Kouchoukos, M.R. Moon, T.M. Sundt 3rd: The influence of mechanical properties on wall stress and distensibility of the dilated ascending aorta, J Thorac Cardiovasc Surg. 126(3), 2003, pp.842-850.

[26] C.J. Beller, M.R. Labrosse, M.J. Thubrikar, F. Robicsek, "Role of aortic root motion in the pathogenesis of aortic dissection", Circ. 109, 2004, pp.763-769.

[27] D. Angouras, D.P. Sokolis, T. Dosios, N. Kostomit- sopoulos, H. Boudoulas, G. Skalkeas and P.E. Karayannacos, "Effect of Impaired Vasa Vasorum Flow on the Structure and Mechanics of the Thoracic Aorta: Implications for the Pathogenesis of Aortic Dissection", Eur. J. Cardio-Thorac. Surg., 17, 2000, pp.468–473.